METAL PAD VELOCITY MEASUREMENTS BY THE IRON ROD METHOD

Brian F. Bradley,   Ernest W. Dewing,   and   John N. Rogers

Alcan International Ltd. Alcan International Ltd. Present Address:
Chalfont Park   P.O. Box 8400   Autosense Equipment Ltd.
Gerrards Cross   Kingston, Ontario   United Technologies Corp.
Buckinghamshire   Canada K7M 5T8   Station Approach
England SL9 0QB   Bicester, Oxfordshire
                                                  England OX6 7BZ

The rate of dissolution of iron rods in aluminum was determined as a function of velocity at 955°C. The results appeared at first to be in disagreement with earlier work by Johnson (1) at lower temperatures, but it seems that it is the temperature coefficient which is at fault. All the results available have been fitted to

$$v(cm\ s^{-1}) = 8.38 \times 10^{-4}\ \delta D\ \exp\ (13410/T) - 3.8$$

where δD is the decrease in diameter (cm) of an initally 9.5 mm (3/8 in.) rod in 7 min immersion at temperature T (K). Calculated values of $v > 25\ cm\ s^{-1}$ are unreliable.

Measurements in cells at the Invergordon Smelter of what was then the British Aluminium Co. showed that speeds in the upstream half of the cells were generally higher (1.4:1) than in the downstream half, with the highest speeds in the upstream corners. These are the points at which those cells tended to tap out. The flow in the upstream halves generally reversed direction as the cells aged, in association with the growth of a freeze toe on the cathode and a change in the horizontal currents in the metal pad.

Introduction

In 1978 Johnson (1) published a method for determining the rate and direction of metal flow in a reduction cell. It involved putting an iron rod vertically into the cell for a given period of time and observing the dissolution. He reported his calibration results (obtained by moving the rods in a pool of metal) in terms of a mass-transfer coefficient, k, which he defined by

$$k = \delta D/(2t\ \ell n[1 + (x_o - x_B)/(1 - x_o)]) \qquad (1)$$

where δD is the reduction of diameter of the rod in time t, x_o is the equilibrium (saturated) mole fraction of Fe in Al at the temperature in question, and x_B is the mole fraction of iron in the bulk of the aluminum in which dissolution is taking place. Johnson also fitted his results to the dimensionless equation

$$Nu = A + B\ Re^n\ Sc^m \qquad (2)$$

where

Nu = Nusselt number for mass transfer = $\dfrac{k\bar{d}}{D}$

Re = Reynolds number = $\rho\ \dfrac{U\bar{d}}{\mu}$

Sc = Schmidt number = $\dfrac{\mu}{\rho D}$

A, B, n, m = constants

k = mass transfer coefficient (cm s^{-1})

$\bar{d}$ = average rod diameter (cm)

D = diffusivity of iron in aluminum ($cm^2\ s^{-1}$)

U = metal velocity (cm s^{-1})

ρ = density of molten aluminum (g cm^{-3})

μ = kinematic viscosity of molten aluminum (g $cm^{-1}\ s^{-1}$)

The values he found for the constants were A = 2.0, B = 0.00853, n = 0.72, and m = 0.36. Although it is not immediately obvious, the resulting equation gives a calibration for all temperatures, since the viscosity, diffusivity, iron solubility, and density are functions only of the temperature. Indeed, none of these quantities is an independent variable; all change at once. Thus the significance of the analysis in terms of dimensionless numbers is not clear, and it only serves to reproduce the experimental temperature coefficient. It should be noted that the equation applies in any case only to rods of 3/8 in. diameter; Johnson remarks that for 5/8 in. rods it does not work, indicating thereby some limitation in the theoretical basis.

We have made new calibration measurements, at a higher temperature than Johnson, have fitted all the results to one equation, and have made measurements in operating cells.

Calibration

Iron rods were obtained from SKF Steel; Table I shows the analysis. Diameter was 3/8 in. (9.52 mm). Calibration was done by mounting two rods in a rotating rig (Figure 1) and immersing them in molten aluminum in a 0.5 ton furnace. It is assumed that the metal remained stationary and was not stirred around by the rods· The background concentration of iron built up (< 0.5%) was low enough not to affect the rate of dissolution.

Table I. Analysis of Iron Rods

Element	wt%	Element	wt%
C	0.03	Cr	0.05
Si	0.05	Ni	0.08
Mn	0.18	Cu	0.05
P	0.01	Sn	0.01
S	0.02		

Standard time of immersion was 7 min, and the temperature was 955 ± 10°C. After removal, the rods were cleaned in strong caustic solution for 24 h. Measurements were made as indicated in Figure 2, and Figure 3 shows a plot of reduction in diameter against velocity. Some results from Johnson (1) are shown for comparison.
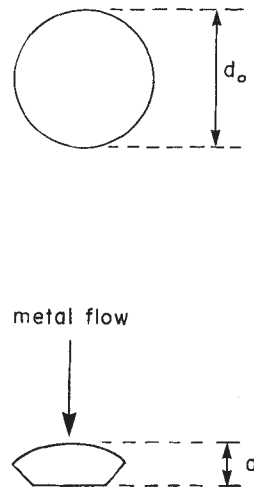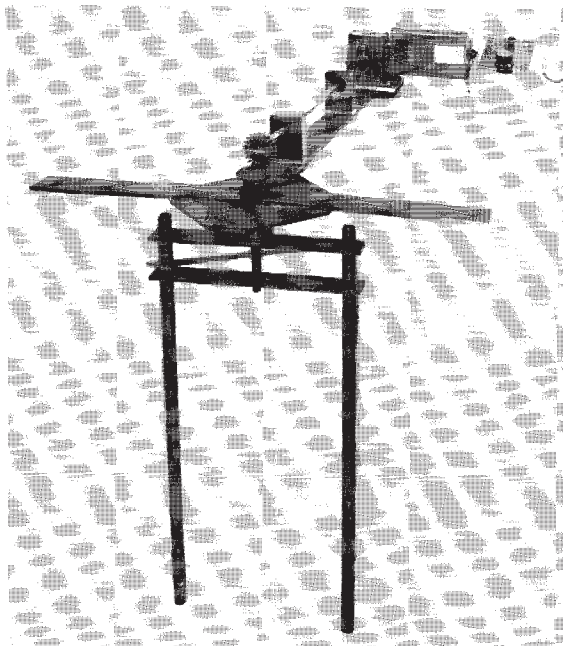

Figure 1 – Rotating rig for calibrating rod dissolution rate.

Figure 2 – Cross section of rod before and after immersion (schematic).
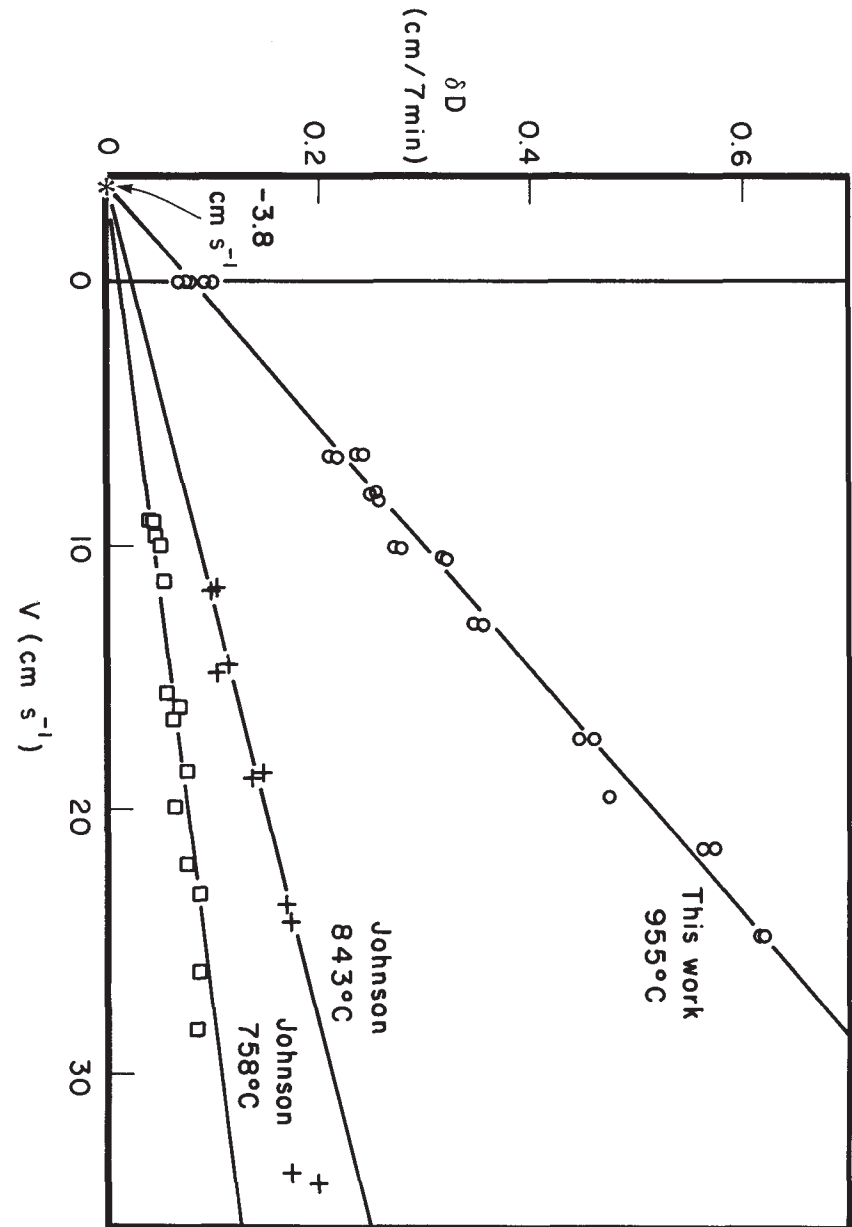

Figure 3 – Reduction of diameter in 7 min vs flowrate.

It is surprising that a simple linear relationship should emerge between the diameter of a rod after dissolution and the speed at which it was rotated through the metal, at least up to 25 cm s^{-1}. The mechanism for iron dissolution in aluminum is complicated, since several Al-Fe phases are formed at the interface and the removal of the dissolved iron from the interface depends on both diffusion and bulk mass transfer rates. In addition, the area and shape of the rod presented to the aluminum changes during the dissolution period. In view of the complexity involved, no theoretical interpretation of the rate of dissolution has been attempted. However, it should be noted that the viscosity of aluminum, and the solubility and diffusivity of iron in it, all follow relations of the type

$$\log x = C/T + D \qquad (3)$$

where T is the temperature in kelvin. One might thus anticipate that, for a given velocity, the rate of dissolution would follow a similar law.

The least-squares straight lines representing the results at the various temperatures all have negative intercepts on the velocity axis (i.e. dissolution is still observed at zero velocity). Statistically the intercepts do not differ significantly one from another, and the best value is −3.8 cm s^{-1}. All the lines have been passed through that point, and the slopes are plotted in Figure 4. Equation (3) is seen to work well; the line has been drawn through the point at 955°C, partly because there are more measurements at that temperature than any other, and partly because it is closest to the temperature of prime interest. The results can now be given as

$$v(cm\ s^{-1}) = 8.38 \times 10^{-4}\ \delta D \exp (13410/T) - 3.8 \qquad (4)$$

where, it must be remembered, T is temperature in kelvin, and δD is the dissolution observed in 7 minutes immersion. If a different immersion time is used, then δD must be scaled pro rata. This equation only works up to v ≃ 25 cm s^{-1}; beyond that Figure 3 suggests that the rate of dissolution becomes almost independent of velocity.

Measurements on Cells

Figure 5 shows a schematic layout of the 130 kA Invergordon cell. It was found that the flow could be characterized by meaurements at eight or ten standard positions, as indicated. Because of fume emission regulations, only one side hood could be removed from a cell at one time. It took about an hour to measure the ten points, and the first measurement was generally repeated to check that the flow was unchanged. The check results usually agreed to within 10% in the speed and 10° in the direction.

To insert the rods, holes about 5 cm diameter were broken in the crust. The rods were dropped in rapidly to prevent bath freezing on them on the way down. Each rod had a flat filed on it at the top, and this flat was oriented to be parallel to the side of the cell.

Measurements were made in 20 different cells; in two of them 7 sets of measurements were made over a period of 2 years. Table II gives a summary of the results.
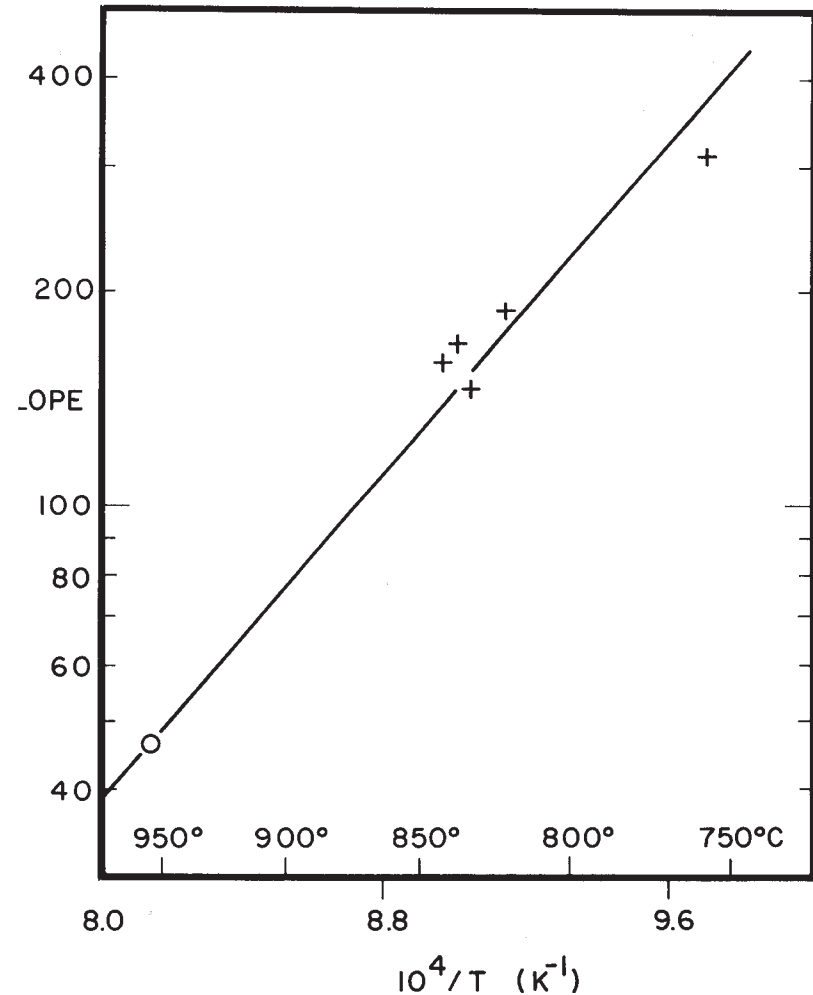

Figure 4 - Slope of lines in Figure 3 as a funcion of temperature.

Table II. Summary of Velocity Measurements

Age of Cell (days)	Number of Cells	Average Speed (cm/s)	Standard Deviation (cm/s)	Ratio Velocities Upstream/ Downstream	Standard Deviation	Maximum Speed (cm/s)	% Readings over 20 cm/s
<150	10	12.0	2.4	1.6	0.46	27.2	15.8
150-400	10	11.6	2.0	1.4	0.36	22.9	6.2
400-900	19	10.6	1.9	1.3	0.39	25.9	2.6
>900	15	11.4	1.9	1.3	0.55	27.4	4.4
All	54	11.3	2.0	1.4	0.45		

Young cells all had similar flow patterns, but there were wide variations in the flow in older cells. Because of these variations the cells were divided into four arbitrary age groups, and the flows for all cells in a group were combined. The averaged flow patterns are shown in Figures 6-7. There are two important points to be emphasized:

(a) Only for the new cells (< 150 days) can the flow be characterized with any certainty. In all the other age groups there is a wide variation in pattern.

(b) This variation is largest for the cells in the 400-900 days group. As a result, the vectorically average flow gives the impression that the velocities are generally low. This is not the case; in fact the average speed is almost independent of age.

The new cells have a vortex at each end. The metal speeds are higher on the upstream side, and are largest at the corners. A central ridge is generally present on the cathode under the crustbreaker, and this may be high enough to partially divide the metal. There is then a vortex in both upstream corners, the vortices at opposite ends having opposite direction of rotation. The pattern in the downstream half of the cell is less clear, but there is basically again a vortex in each corner. The direction of these downstream vortices varied from cell to cell.

The group of young cells (150-400 days) showed a pattern similar to, but less distinct than, that seen for the first set. The highest speeds were still in the vortices at the upstream corners. No general pattern could be deduced for the flow in the downstream half of the cell. The upstream speeds were still larger than those downstream, but the difference was less marked than in the new cells.

The middle-aged cells (400-900 days) showed greater variations than the two previous groups, with each cell having its own pattern. On averaging the velocities, therefore, no general pattern emerged.

The group of old cells (> 900 days) again showed wide variations, but a clear trend could be seen when the velocities were averaged. Again there was a vortex in each of the upstream corners, but the directions were opposite from those in the new cells. On the downstream side there appeared to be a vortex in one corner, but no pattern could be discerned in
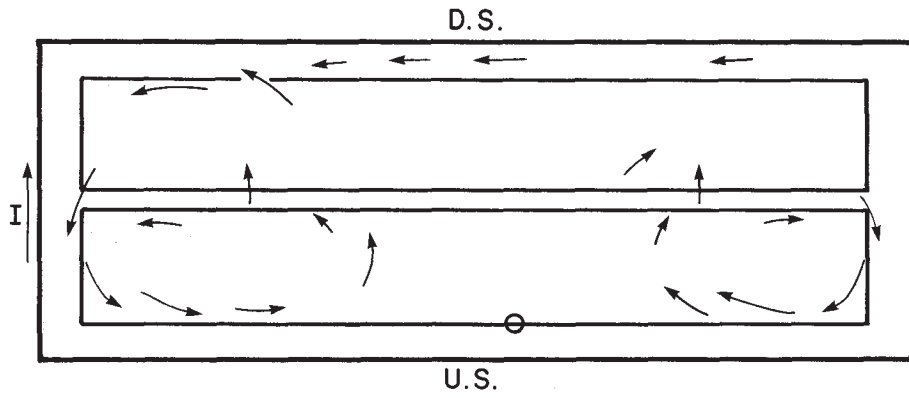

Base of Cathode
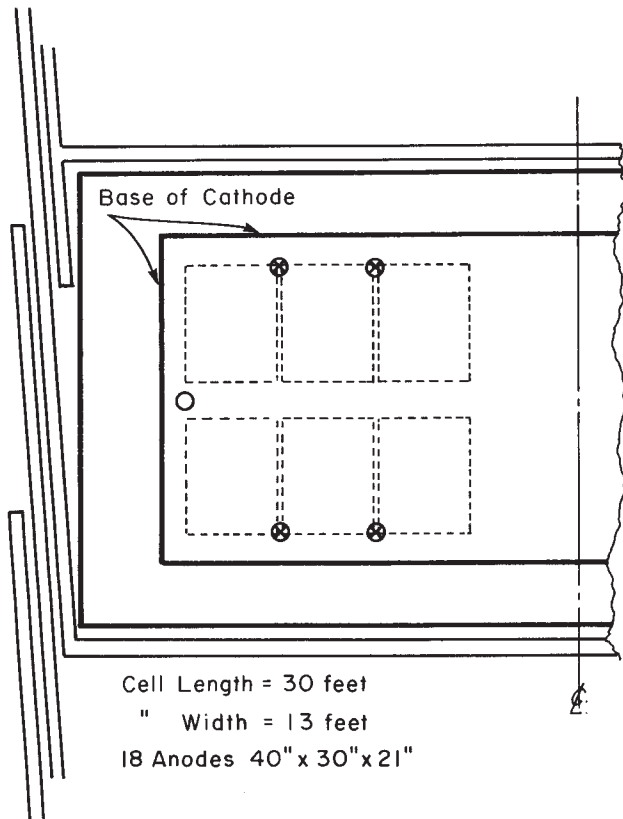
Cell Length = 30 feet
"   Width = 13 feet
18 Anodes 40"x 30"x 21"

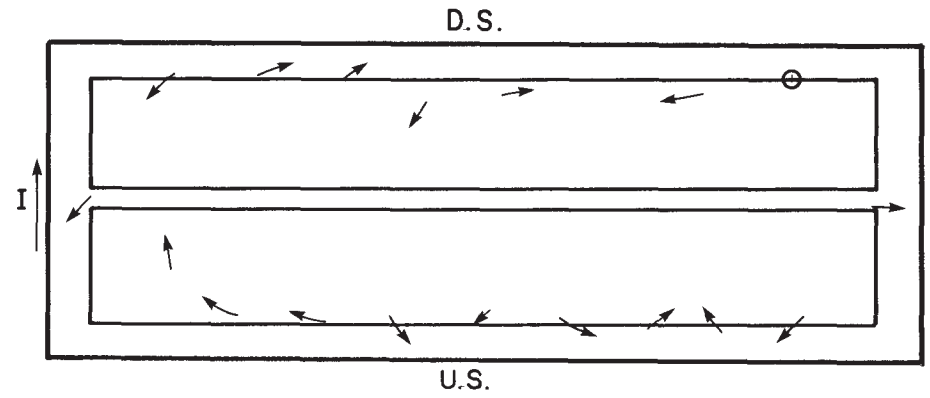⊗ = STANDARD POINTS FOR IRON ROD IMMERSION FOR METAL FLOW READINGS

○ = SUBSIDARY POINTS.

Figure 5 – Schematic layout of Invergordon cell.

METAL FLOW IN CELLS <150 DAYS OLD

D.S.

U.S.

O= NO CONSISTENT FLOW PATTERN - VELOCITIES LOW

METAL FLOW IN CELLS 400-900 DAYS OLD

D.S.

U.S.

O= NO CONSISTENT FLOW PATTERN - VELOCITIES LOW
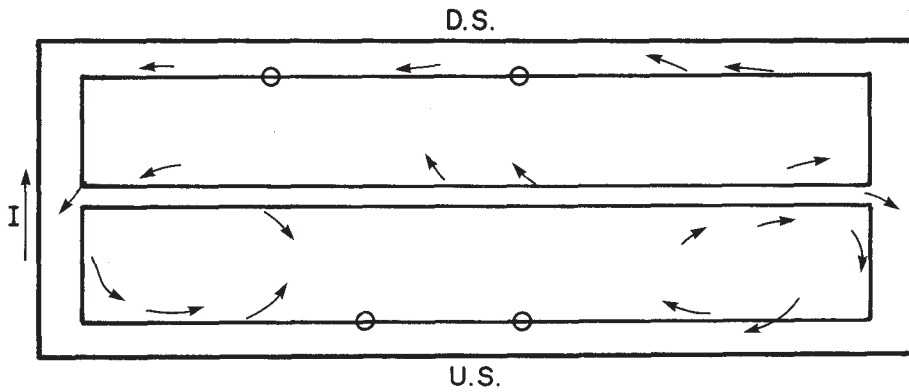
METAL FLOW IN CELLS 150-400 DAYS OLD

D.S.

U.S.

Figure 6 - Flow patterns.
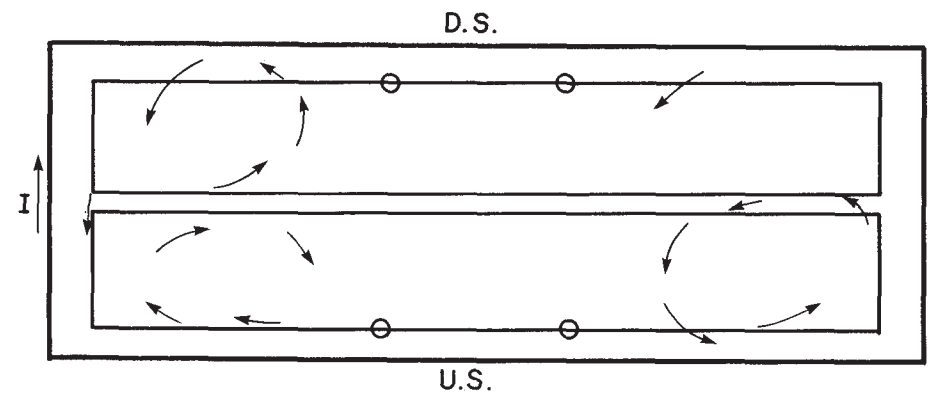
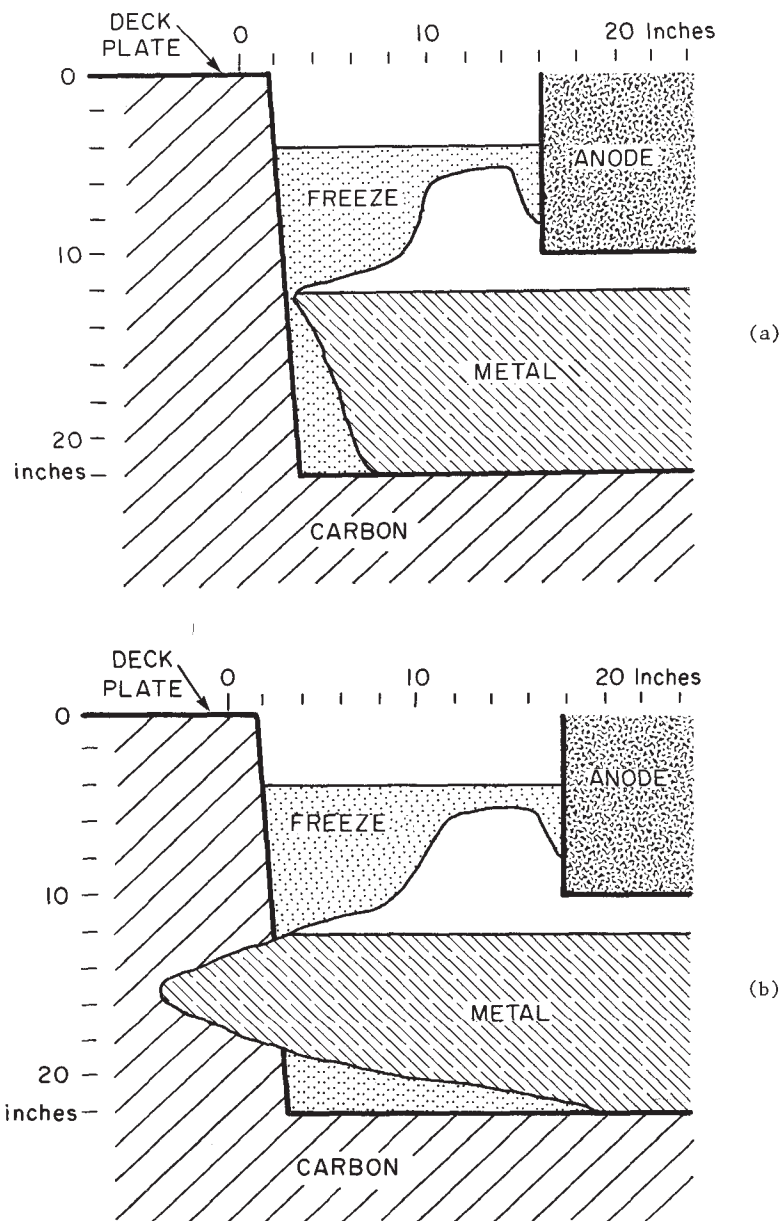METAL FLOW IN CELLS >900 DAYS OLD

D.S.

U.S.

Figure 7 - Flow patterns.

(a)

(b)

Figure 8 - Freeze profiles (a) <150 days (b) >900 days.

the other. There was again an appreciable difference between the upstream and downstream speeds.

Overall the average metal speed along the anode edge was 11 cm s^{-1}, and the ratio of upstream to downstream velocity was 1.4.

The average trends with age given above were also seen in the two cells followed over 2 years. The first showed the flow characteristic of a new cell when first measured at 62 days, changed to that of a young cell (as seen at 277 days) and to a less well defined pattern (492, 612 and 800 days). Similarly, the other cell initially showed the uncharacterized pattern of a middle-aged cell (527, 735 and 807 days), but as it exceeded 900 days the pattern became established at that expected in an old cell (950, 1031, 1101 and 1283 days).

Discussion

Quite apart from a 'neck' in the iron rod at the level of the metal-bath interface, the velocities derived from measurements of the diameter at the top and the bottom of the metal pad often showed large differences.

The flows measured a week apart in the same cell showed little basic change in pattern, despite larger differences in the anode current distribution. This is not surprising, as localized changes in the forces might produce little change in the overall pattern, which is determined by the forces over a large area.

The positions of greatest change in metal momentum (and hence presumably in sidewall erosion) were at the upstream corners, and in particular at the upstream sides of the endwalls. An examination of the records shows that more cells tapped out at the endwalls than elsewhere, and the age of failure at these points was less than that due to other tap outs. Also more cells tapped out upstream than downstream, and at a younger age.

The shape of the freeze on the sidewalls was measured in about a dozen cells. The measurements showed large differences from cell to cell and, for the older cells, from point to point in the cell. It was also found that the freeze profile could change rapidly with time (e.g. before and after an anode effect). This was particularly true of the freeze toe on the cathode in old cells. Typical results are shown in Figure 8. The major changes with age were the undercutting of the sidewall near the metal-bath interface and the growth of a ledge (or toe) on the cathode which could extend under the anode shadow. It was perhaps the effect of this insulating freeze toe on the distribution of horizontal current in the metal pad which was responsible for the change of circulation pattern with age.

Acknowledgements

References

(1) A.R. Johnson, "Metal Pad Velocity Measurements in Aluminum Reduction Cells", AIME Light Metals, 1978.